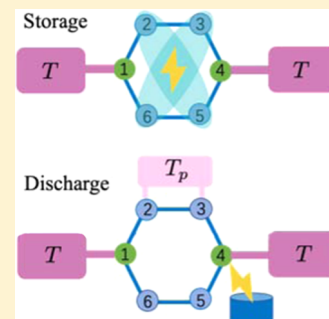


Loss-Free Excitonic Quantum Battery

Junjie Liu,^{*,†,‡} Dvira Segal,[‡] and Gabriel Hanna^{*,†}[†]Department of Chemistry, University of Alberta, Edmonton, Alberta T6G 2G2, Canada[‡]Department of Chemistry and Centre for Quantum Information and Quantum Control, University of Toronto, Toronto, Ontario M5S 3H6, Canada

ABSTRACT: Robust quantum energy storage devices are essential to realize powerful next-generation batteries. Herein, we provide a proof of concept for a loss-free excitonic quantum battery (EQB) by using an open quantum network model that exhibits exchange symmetries linked to its structural topology. By storing electronic excitation energy in a symmetry-protected dark state living in a decoherence-free subspace, one can protect the charged EQB from environment-induced energy losses, thereby making it a promising platform for long-term energy storage. To illustrate the key physical principles and potential functionality of this concept, we consider an open quantum network model of a *para*-benzene-like structure. We demonstrate through numerical simulations the immunity of the charged EQB to environmentally induced losses and further show how to harness the stored energy by adding a symmetry-breaking perturbation (SBP) to the network. We also investigate the impact of static disorder and temperature fluctuations of the SBP on the performance of the EQB during its storage and discharge phases. Apart from the cases with very strong static disorder, the performance of the EQB is essentially unaltered, thereby demonstrating the robustness of the proposed EQB.



1. INTRODUCTION

Growth in the global demand for renewable energies has intensified the need for robust and efficient batteries for energy storage.^{1–4} Indeed, over the last several decades, significant progress has been made in battery technologies based on classical electrochemical working principles, which are now in wide use. More recently, there has been a great interest in developing a new class of batteries, known as quantum batteries (QBs), whose operation relies on quantum mechanical working principles.^{5–17} By exploiting genuinely quantum effects, the desire has been to devise batteries with unique properties, capable of outperforming their conventional classical analogues.

Although considerable efforts have been devoted to designing strategies for maximizing the stored energy and average charging power of QBs,^{7–9} the microscopic models used to study them have been primarily based on closed quantum systems following unitary dynamics. However, it is inevitable that a quantum system will interact with its surrounding environment, thereby suffering decoherence and dissipation processes.^{18–20} Such processes can have detrimental effects on a system's quantum coherences and quantum correlations, which are crucial resources for QBs.^{5–9} Hence, any realistic modeling of QBs must accurately take into account open-system effects. Very recently, an important step in this direction was taken in refs 14 and 21, in which a QB device was modeled as an open quantum system during its charging process.

From a practical standpoint, a logical step forward would be to now consider a charged QB during the storage phase as an open quantum system. Throughout this phase, open charged QBs are expected to experience fluctuations and dissipation due to their coupling to the surrounding environments. Therefore, to achieve long-time energy storage in real QBs, one must design

open QBs that are resistant to decoherence and energy loss over time.

The use of quantum states that are less sensitive to environmental perturbations to achieve passive protection of quantum resources has a long history in the field of quantum information processing.²² A prominent example is that of a decoherence-free subspace (DFS), i.e., a subspace of the system's Hilbert space inside which the dynamics is purely unitary.^{23–29} As a result of this property, DFSs have emerged as useful structures for the preservation of quantum information. Despite the conceptual differences between the protection of quantum information and storage of energy, herein, we will show that DFSs can be used to develop a passive protection scheme for charged QBs.

In this study, we focus on an excitation energy storage device as a platform for an open charged QB and model it in terms of an open quantum network (OQN). Previously, OQNs have been used in studies of excitation energy transfer (EET) in natural and artificial photosynthetic complexes.^{30–34} To introduce a passive protection scheme, we consider OQNs exhibiting exchange symmetries linked to their structural topologies. Owing to the symmetries, we show that these OQNs can host dark states (DSs) living in DFSs and that the invariant nature of the DSs, in principle, allows one to eliminate energy losses due to dissipation. In other words, the use of symmetry-protected DSs effectively decouples the battery from its environments, making it possible to perfectly store the excitation energy. This setup gives rise to the concept of a loss-free excitonic QB (EQB). Therefore, in contrast to conventional electrochemical batteries,

Received: July 4, 2019

Published: July 7, 2019

this charged EQB does not “discharge” over time in the presence of environments, a remarkable feature stemming from the quantum nature of the system. A stable QB based on a three-level system has been recently proposed in ref 35, a design which bears some resemblance to our loss-free EQB. However, this proposal relies on slowly varying (adiabatic) driving fields and exploits the stimulated Raman adiabatic passage protocol³⁶ to ensure adiabatic evolution of a dark state, in direct contrast to our symmetry-protected scheme. To harness the stored energy, we couple the EQB to a symmetry-breaking perturbation (SBP). Breaking the structural symmetry effectively restores the coupling of the system to its environments, thereby allowing excitonic energy to flow out of the EQB toward the exit site of the network and ultimately to be utilized.

To understand the impact of structural imperfections and their effects on the exchange symmetry on the performance of the proposed EQB, we study the effects of static disorder on the EQB in both the storage and discharging phases, i.e., without and with the SBP, respectively. We find that when the EQB is subject to a diagonal (local site energy) disorder during its storage phase, energy leakage occurs but only under a significant level of disorder. On the other hand, when the EQB is subject to an off-diagonal disorder during its storage phase, we observe redistribution of the stored energy within the battery, along with an insignificant amount of energy leakage. Remarkably, the discharging process is unaffected by (even a pronounced) static disorder. We attribute the robustness of the discharging efficiency to the fact that the SBP already completely breaks the structural symmetry, making the EQB essentially insensitive to fluctuations in the on-site energies and nearest-neighbor electronic couplings. We also consider the role of temperature fluctuations of the SBP, which could occur due its finite size. We find that the EQB essentially maintains its ideal functionality under small temperature fluctuations. These studies highlight the utility of a loss-free EQB.

The paper is organized as follows. First, in Section 2, we present the general framework for modeling open EQBs in terms of OQNs. We then introduce an exchange symmetry, which allows the OQNs to host DFSs and DSs, and describe the underlying working principle of a loss-free EQB. In Section 3, we present a proof-of-concept illustration based on a minimal model of an open EQB and demonstrate the robustness of this EQB with detailed simulations under various conditions in Section 4. We summarize our observations in Section 5.

2. GENERAL FRAMEWORK

2.1. Modeling an Open Quantum Battery. To lay down the general framework for the loss-free EQB, we consider EET of a single Frenkel exciton^{37–39} in an OQN with N sites. The Hilbert space of the network itself is spanned by the site basis states $\{|n\rangle\}$, where each state corresponds to the excitation being localized on site n . In this site basis, the network can be described in terms of the following Hamiltonian (setting $\hbar = 1$)

$$\hat{H}_N = \sum_{n=1}^N E_n |n\rangle\langle n| + \sum_{n \neq m} J_{n,m} |n\rangle\langle m| \quad (1)$$

where E_n is the on-site energy of site n and $J_{n,m}$ is the excitonic coupling strength between sites n and m . Here, we adopt a single-excitation manifold for describing the EET in the OQN and thus the EQB is limited to storing one exciton at a time. The single-excitation manifold is commonly used in the study of EET in light-harvesting complexes due to the fact that exciton

recombination is typically much slower (on the order of nanoseconds) than the exciton transfer times (on the order of picoseconds).^{30,40} One can further generalize the present theoretical framework to systems involving multiple-excitation manifolds,³⁹ thereby increasing the energy storage density.

In our open network, selected (outer) sites are coupled to heat baths; we refer to these sites as surface sites (SSs). The remaining (interior) sites do not directly interact with the surrounding environment, and they are referred to as bulk sites (BSs). The sum of the bath and network–bath interaction Hamiltonians is given by

$$\hat{H}_B + \hat{H}_{NB} = \frac{1}{2} \sum_{n \in \text{SSs}} \sum_j^M \left[\hat{p}_{n,j}^2 + \omega_{n,j}^2 \left(\hat{R}_{n,j} - \frac{C_{n,j}}{\omega_{n,j}^2} |n\rangle\langle n| \right)^2 \right] \quad (2)$$

Here, each SS is coupled to an independent bosonic heat bath containing M oscillators at a temperature T , with $\hat{P}_{n,j}$, $\hat{R}_{n,j}$, and $\omega_{n,j}$ as the mass-weighted momentum, position, and frequency of the j th oscillator, respectively, and $C_{n,j}$ as the network–bath coupling coefficient between the n th SS and j th oscillator of the attached heat bath. We assume the EQB to be in a factorized initial state $\hat{\rho}_{\text{tot}}(0) = \hat{\rho}_N(0) \otimes \hat{\rho}_B(0)$, where $\hat{\rho}_N(0)$ is the initial state of the network and $\hat{\rho}_B(0) \propto e^{-\beta \hat{H}_B}$ is the initial bath state, taking a canonical form characterized by an inverse temperature $\beta \equiv 1/T$ (setting $k_B = 1$). The bath frequencies, $\{\omega_{n,j}\}$ and coupling coefficients, $\{C_{n,j}\}$ are determined by a spectral density, assumed to be identical for all SSs, of a Debye–Drude form $J(\omega) = 2\lambda_b \frac{\omega\omega_c}{\omega^2 + \omega_c^2}$, where λ_b is the bath reorganization energy and ω_c is the cut-off frequency.⁴¹

2.2. Exchange Symmetry and Working Principle. We now focus on OQNs that possess exchange symmetries linked to their structural topologies, as characterized by a unitary symmetry operator $\hat{\Pi}$, satisfying

$$[\hat{\Pi}, \hat{H}_N] = 0, \quad [\hat{\Pi}, |n\rangle\langle n|] = 0 \quad \forall n \in \text{SSs} \quad (3)$$

i.e., $\hat{\Pi}$ generates invariant permutation operations between BSs of the OQN. We denote by $\{|\psi_\alpha^{(k)}\rangle\}$ and $\{u_\alpha\}$ the eigenstates and eigenvalues of $\hat{\Pi}$, respectively, where $\alpha = 1, 2, \dots, L$ ($L \geq 1$) and k can take the values $1, \dots, d_\alpha$ ($d_\alpha \geq 1$). Here, L is the number of distinct eigenvalues of $\hat{\Pi}$ with $1 \leq L \leq N$ and d_α is the dimension of the eigenspace corresponding to the eigenvalue u_α satisfying $\sum_{\alpha=1}^L d_\alpha = N$. Since \hat{H}_N and $\hat{\Pi}$ share a common eigenbasis according to eq 3, we may decompose the Hilbert space \mathcal{H} of the OQN as

$$\mathcal{H} = \bigoplus_{\alpha=1}^L \mathcal{H}_\alpha \quad (4)$$

where $\mathcal{H}_\alpha = \{|\psi_\alpha^{(k)}\rangle, k \in [1, d_\alpha]\}$ and the corresponding operator space $\mathcal{B}(\mathcal{H})$ is

$$\mathcal{B}(\mathcal{H}) = \bigoplus_{\alpha=1}^L \bigoplus_{\alpha'=1}^L \mathcal{B}_{\alpha\alpha'} \quad (5)$$

where $\mathcal{B}_{\alpha\alpha'} = \{|\psi_\alpha^{(n)}\rangle\langle\psi_{\alpha'}^{(m)}|, n \in [1, d_\alpha], m \in [1, d_{\alpha'}]\}$ and has the dimension $d_\alpha d_{\alpha'}$. One can show that the existence of $\hat{\Pi}$, together with the properties in eq 3, guarantees that the composite dynamics generated by the total Hamiltonian $\hat{H}_N + \hat{H}_B + \hat{H}_{NB}$ leaves the $\mathcal{B}_{\alpha\alpha'}$ subspaces invariant;⁴² i.e., an operator belonging to the operator subspace $\mathcal{B}_{\alpha\alpha'}$ cannot be mapped onto operators in other subspaces during the time evolution generated by the total Hamiltonian.

Among the diagonal operator subspaces $\{\mathcal{B}_{\alpha\alpha}\}$, in which physical density matrices with unit trace live, one-dimensional subspaces $\mathcal{B}_{\alpha\alpha} = |\psi_{\alpha}^{(1)}\rangle\langle\psi_{\alpha}^{(1)}|$, i.e., diagonal subspaces with $d_{\alpha} = 1$, are of particular appeal because the dynamics maps them onto themselves. Such subspaces, also known as DFSs, have proven useful in the fields of quantum information and quantum computing for preventing dissipation and dephasing due to the interaction with the environment.^{23,24,26,28,43–49} The state $|\psi_{\alpha}^{(1)}\rangle$ is known as a dark state (DS). Owing to a DS's immunity to environmental effects, a sensible charging protocol for the EQB would then be to initialize the OQN in one of its symmetry-allowed DSs, i.e., $\hat{\rho}_{\text{N}}(0) = |\psi_{\alpha}^{(1)}\rangle\langle\psi_{\alpha}^{(1)}|$. Experimentally, the stimulated Raman adiabatic passage technique may be used to prepare dark states.³⁶ As the dynamical generator of the composite dynamics will leave $|\psi_{\alpha}^{(1)}\rangle\langle\psi_{\alpha}^{(1)}|$ invariant, we should have $\hat{\rho}_{\text{N}}(t) = |\psi_{\alpha}^{(1)}\rangle\langle\psi_{\alpha}^{(1)}|$ as well. Therefore, the excitation energy stored in the initial DS will be protected against bath-induced dissipation processes as long as the exchange symmetry of the OQN is maintained.

To discharge the EQB, we introduce a SBP onto the network. As a result, the reduced density matrix leaves the dark-state subspace, i.e., $\hat{\rho}_{\text{N}}(t) \neq |\psi_{\alpha}^{(1)}\rangle\langle\psi_{\alpha}^{(1)}|$. As we will show later, the application of the SBP causes the excitation energy stored in the initial DS to be transferred from the bulk sites to the surface sites and eventually out to a sink connected to one of the SSs (termed the exit site). Here, the SBP (denoted by P for perturbation) is represented by a set of M harmonic oscillators and the network–SBP interaction Hamiltonian is assumed to have a bilinear form,⁵⁰ such that

$$\hat{H}_{\text{P}} + \hat{H}_{\text{NP}} = \frac{1}{2} \sum_k^M \left[\hat{p}_k^2 + \Omega_k^2 \left(\hat{r}_k - \frac{\gamma_k}{\Omega_k^2} \hat{S} \right)^2 \right] \quad (6)$$

where \hat{S} is a network operator consisting of projection operators $|n\rangle\langle n|$ with $n \in \text{BSs}$ (the exact form of S is chosen in such a way that the exchange symmetry is completely broken by the SBP). Here, \hat{p}_k , \hat{r}_k , and Ω_k are the mass-weighted momentum, position, and frequency of the k th oscillator, respectively, and γ_k is the coupling strength between the k th oscillator of the SBP and the network. The bilinear coupling to the SBP is characterized by a Debye–Drude spectral density $J(\omega) = 2\lambda_{\text{p}} \frac{\omega\omega_{\text{p}}}{\omega^2 + \omega_{\text{p}}^2}$, where λ_{p} is the reorganization energy and ω_{p} is the cut-off frequency (λ_{p} should be small as the SBP simply acts as perturbation to the EQB). When including the SBP, the initial condition for the composite system should be $\hat{\rho}_{\text{tot}}(0) = \hat{\rho}_{\text{N}}(0) \otimes \hat{\rho}_{\text{B}}(0) \otimes \hat{\rho}_{\text{P}}(0)$, where $\hat{\rho}_{\text{P}}(0) \propto e^{-\beta_{\text{p}}\hat{H}_{\text{P}}}$ assumes a canonical form characterized by an inverse temperature $\beta_{\text{p}} \equiv 1/T_{\text{p}}$. In this case, we only consider the effect of a single SBP but the general conclusions are expected to be the same when multiple SBP elements (each of which acts locally on a BS) are used.

Given the excitonic nature of the QB, which stores excitons and the associated excitation energy, it is meaningful to use the so-called transfer efficiency of the EET to monitor the performance of the EQB during the storage and discharging stages. The transfer efficiency is defined as the population transferred to the sink due to an irreversible trapping process (with a rate κ) from the exit site of the network,^{30,51} i.e.

$$\eta(t) = 2\kappa \int_0^t \langle e|\hat{\rho}_{\text{N}}(t')|e\rangle dt' \quad (7)$$

where $\langle e|\hat{\rho}_{\text{N}}(t)|e\rangle$ is the population at the exit site and the trapping rate, κ , is set to 1 ps^{-1} , which is typical for EET population transfer dynamics.⁵²

3. PROOF OF CONCEPT

3.1. Model. To illustrate the key features of the proposed EQB, we consider an OQN model of a *para*-benzene-like structure coupled to two heat baths (see inset of Figure 1a for an

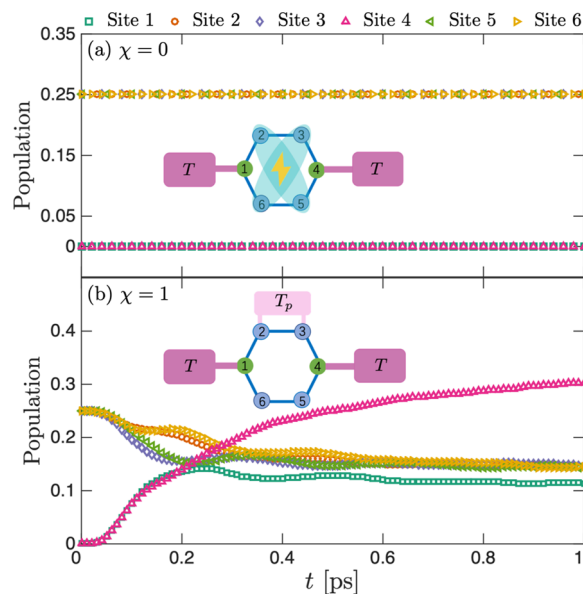


Figure 1. Time-dependent site populations for the OQN during (a) storage (without the SBP, $\chi = 0$) and (b) discharge (with an SBP that is coupled to sites 2 and 3, $\chi = 1$). Results for sites 1, 2, 3, 4, 5, and 6 are represented by squares, circles, diamonds, upward-pointing triangles, left-pointing triangles, and right-pointing triangles, respectively. The insets illustrate the setups used in the simulations. A time step of $\Delta t = 1$ fs and an ensemble of 1×10^4 trajectories are used to obtain converged DECIDE results. The bath and SBP parameters are chosen as $T = 300$ K, $T_{\text{p}} = 300$ K, $\lambda_{\text{b}} = 35 \text{ cm}^{-1}$, $\lambda_{\text{p}} = 10 \text{ cm}^{-1}$, $\omega_{\text{c}} = \omega_{\text{p}} = 106 \text{ cm}^{-1}$, $\omega_{\text{max}} = 50\omega_{\text{c}}$, and $M = 100$.

illustration of the network). We emphasize that in this work, we do not attempt to realize the proposed idea using molecular systems. Rather, as suggested in ref 35, the EQB could be realized using artificially engineered systems, e.g., superconducting units. The quantum network is described by the following Hamiltonian

$$\hat{H}_{\text{N}} = \sum_{n=1}^6 E_n |n\rangle\langle n| + h \sum_{\langle n,m \rangle} |n\rangle\langle m| \quad (8)$$

where E_n is the on-site energy of site n , h is the nearest-neighbor electronic coupling strength, and the sum over $\langle n, m \rangle$ is carried out over nearest-neighbor sites with cyclic boundary conditions. We note that in Hückel's theory for a benzene molecule,^{42,53} $E_n = \varepsilon$ for all n . However, in our model, the quantum network is coupled to heat baths (through the SSs) and the on-site energies of the SSs are in general different from each other and from those of the BSs. Here, we adopt the following configuration, where sites 1 and 4 are the SSs and site 4 is the exit site (the numbering convention can be found in the inset of Figure 1a).

In the absence of the SBP, the OQN exhibits exchange symmetry generated by the following unitary operator

$$\hat{\Pi} = \exp[i(|2\rangle\langle 6| + |6\rangle\langle 2|)] \otimes \exp[i(|3\rangle\langle 5| + |5\rangle\langle 3|)] \quad (9)$$

which corresponds to two independent, yet simultaneous, permutation operations exchanging the states of sites 2 and 6, as well as those of sites 3 and 5, or equivalently, a 180° rotation around the axis connecting sites 1 and 4. After this operation, the structure of the OQN remains unaltered. Due to the existence of this symmetry operator, the system possesses two DFSs with the corresponding DSs $|\psi_\alpha^k\rangle$ and eigenvalues u_α ^{42,50}

$$\begin{aligned} |\psi_1\rangle &= \frac{1}{2}(|5\rangle + |6\rangle - |2\rangle - |3\rangle), \quad u_1 = E_B + h \\ |\psi_2\rangle &= \frac{1}{2}(|3\rangle + |6\rangle - |2\rangle - |5\rangle), \quad u_2 = E_B - h \end{aligned} \quad (10)$$

In the above equation, the reference to k has been omitted because $d_\alpha = 1$. It can be readily checked that $|\psi_1\rangle$ and $|\psi_2\rangle$ are eigenstates of both $\hat{\Pi}$ and \hat{H}_N and that they are annihilated by the network–bath interaction Hamiltonian \hat{H}_{NB} , thereby satisfying a sufficient condition for the existence of a dark state.⁴⁸

As mentioned earlier, the EQB is initialized in a DS so we choose the initial state of the OQN to be

$$\hat{\rho}_N(0) = |\psi_1\rangle\langle\psi_1| \quad (11)$$

with $|\psi_1\rangle$ given by eq 10; $\hat{\rho}_N(0) = |\psi_2\rangle\langle\psi_2|$ is also a valid choice. In the absence of a SBP, the OQN is expected to undergo dissipationless dynamics, leading to a time-independent reduced density matrix, i.e., $\hat{\rho}_N(t) = |\psi_1\rangle\langle\psi_1|$. Accordingly, the site populations, which reflect the distribution of electronic excitation energy across the network, will be

$$\langle\hat{P}_{nm}(t)\rangle = \langle\hat{P}_{nm}(0)\rangle = \begin{cases} 0, & \forall n \in \text{SSs}, \\ \frac{1}{4}, & \forall n \in \text{BSs} \end{cases} \quad (12)$$

where $\hat{P}_{nm} = |n\rangle\langle n|$ is the projection operator of site n , the ensemble average of which defines the site population. In other words, the initially injected electronic excitation energy is uniformly distributed among the four BSs and stored in the bulk states indefinitely. It is worthwhile to mention that the time independence of the site populations results from the exchange symmetry of the OQN only and it does not hinge upon the specific values of the network parameters. To discharge the EQB, we attach to it a SBP and take $\hat{S} = |2\rangle\langle 2| + |3\rangle\langle 3|$ in eq 6, which breaks the exchange symmetry completely (see inset of Figure 1b). With the SBP in place, $|\psi_1\rangle$ is no longer a dark state and therefore over time, population builds up in the SSs, as expected; i.e., the exciton stored within the bulk states is transferred to the SSs.

3.2. Methodology. For open quantum systems with large numbers of degrees of freedom in their environments, full quantum simulations of the composite quantum dynamics are not feasible. Furthermore, in EET systems, the reorganization energy is usually of the same order of magnitude as the electronic coupling, which hinders the utility of perturbative methods such as the Redfield equation. To simulate the quantum dynamics of our OQN with and without the SBP, we employ the recently developed mixed quantum-classical method known as the deterministic evolution of coordinates with initial decoupled equations (DECIDE).⁵⁴ It treats the OQN quantum mechanically and the environment in a classical-like fashion. Previously, it was shown that for the EET dynamics of the Fenna–

Matthews–Olson complex, DECIDE yields results for the time-dependent site populations that are in very good agreement with numerically exact simulations, at both low and high temperatures.⁵⁴ Thus, it is expected that DECIDE could reliably capture the EET dynamics of the OQN model with and without the SBP. DECIDE also provides a computationally tractable way of assessing the impact of weak static disorder in the OQN on the EET dynamics, as it allows one to readily perform thousands of simulations of independent disordered OQN configurations for achieving numerical convergence.

Using the DECIDE method, which relies on a partial Wigner transform^{55,56} over the environments' (viz., thermal baths and the SBP) degrees of freedom, the composite dynamics is governed by the following Weyl-ordered, partially Wigner-transformed Hamiltonian

$$\begin{aligned} \hat{H}_W &= \hat{H}_N + \hat{H}_{NB}(\{R_{n,j}\}) + H_B(\{P_{n,j}\}, \{R_{n,j}\}) \\ &+ \chi[H_p(\{p_k\}, \{r_k\}) + \hat{H}_{NP}(\{r_k\})] \end{aligned} \quad (13)$$

Here, $\{\cdot\}$ denotes a set of bath position or bath momentum variables. The flag χ is either 0 or 1, corresponding to the OQN without or with the SBP, respectively. The generalized coordinates of the OQN are taken to be the $\hat{P}_{nm} = |n\rangle\langle m|$ operators, whereas the coordinates of the thermal baths and SBP are simply their respective position and momentum variables. According to DECIDE, the time evolution of these coupled coordinates is prescribed by the following set of coupled first-order differential equations (FODEs) $d\mathcal{P}_{nm}^{\beta\beta'}(t)/dt = i([\hat{H}_W, \hat{P}_{nm}])^{\beta\beta'}(t)$ and $d\mathbf{X}^{\beta\beta'}(t)/dt = -(\{\hat{H}_W, \mathbf{X}\})^{\beta\beta'}(t)$,⁵⁴ where $[\cdot, \cdot]$ and $\{\cdot, \cdot\}$ are the commutator and Poisson bracket, respectively, $\mathbf{X} = (\{R_{n,j}\}, \{P_{n,j}\}, \chi\{r_k\}, \chi\{p_k\})$ and $\{\beta\} = (11, 12, \dots, 16)$

$$\begin{aligned} \frac{d}{dt}\mathcal{P}_{nm}^{\beta\beta'}(t) &= i[\sum_{l=1}^6 V_{ln}\hat{P}_{lm}(t) - \sum_{v=1}^6 V_{mv}\hat{P}_{nv}(t)]^{\beta\beta'} \\ &- \frac{i}{2}\sum_j C_{n,j}(R_{n,j}(t)\hat{P}_{nm}(t) + \hat{P}_{nm}(t)R_{n,j}(t))^{\beta\beta'}(\delta_{n,1} + \delta_{n,4}) \\ &+ \frac{i}{2}\sum_j C_{m,j}(R_{m,j}(t)\hat{P}_{nm}(t) + \hat{P}_{nm}(t)R_{m,j}(t))^{\beta\beta'}(\delta_{m,1} + \delta_{m,4}) \\ &- \chi\frac{i}{2}\sum_k C_k(R_k(t)\hat{P}_{nm}(t) + \hat{P}_{nm}(t)R_k(t))^{\beta\beta'}(\delta_{n,2} + \delta_{n,3}) \\ &+ \chi\frac{i}{2}\sum_k C_k(R_k(t)\hat{P}_{nm}(t) + \hat{P}_{nm}(t)R_k(t))^{\beta\beta'}(\delta_{m,2} + \delta_{m,3}), \end{aligned}$$

$$\frac{d}{dt}R_{n,j}^{\beta\beta'}(t) = P_{n,j}^{\beta\beta'}(t),$$

$$\frac{d}{dt}P_{n,j}^{\beta\beta'}(t) = -\omega_{n,j}^2 R_{n,j}^{\beta\beta'}(t) + C_{n,j}\hat{P}_{nm}^{\beta\beta'}(t)(\delta_{n,1} + \delta_{n,4}),$$

$$\frac{d}{dt}r_k^{\beta\beta'}(t) = p_k^{\beta\beta'}(t),$$

$$\frac{d}{dt}p_k^{\beta\beta'}(t) = -\Omega_k^2 r_k^{\beta\beta'}(t) + \chi\gamma_k(\hat{P}_{22} + \hat{P}_{33})^{\beta\beta'}(t)$$

(14)

where the coherent coupling is $V_{nm} = E_n + \sum_{j=1}^M C_{n,j}^2/(2\omega_{n,j}^2)(\delta_{n,1} + \delta_{n,4}) + \chi\sum_{k=1}^M \gamma_k^2/(2\Omega_k^2)(\delta_{n,2} + \delta_{n,3})$ with $\delta_{n,m}$ as the Kronecker delta function, and $V_{nm} = h$. Given the completeness condition $\sum_{n=1}^6 \hat{P}_{nn} = 1$, there are $36 \times [35 + 2(2 + \chi)M]$ coupled FODEs for the network, bath, and SBP matrix elements. When $\chi = 0$, the equations of motion for the SBP variables $r_k^{\alpha\alpha'}$ and $p_k^{\alpha\alpha'}$ are decoupled from the rest and therefore we do not need to

propagate them in the simulations. From the above equations of motion, we see that the coordinates of the BSs, SSs, and baths are always coupled, irrespective of the initial conditions of the quantum network. This fact further highlights the open character of the proposed loss-free EQB during the storage phase.

The system–bath coupling coefficients and the frequencies of the bath harmonic oscillators are determined by discretizing the Debye–Drude spectral densities of the baths to yield⁵⁷

$$C_{n,j} = 2\sqrt{\lambda_b \arctan(\omega_{\max}/\omega_c)/(\pi M)} \omega_{n,j} \quad (15)$$

where $\omega_{n,j} = \tan(j \arctan(\omega_{\max}/\omega_c)/M)\omega_c$. Similarly, to simulate the Debye–Drude spectral density of the SBP, the following expression for the system–SBP coupling coefficients is used

$$C_k = 2\sqrt{\lambda_p \arctan(\omega_{\max}/\omega_p)/(\pi M)} \Omega_k \quad (16)$$

where $\Omega_k = \tan(j \arctan(\omega_{\max}/\omega_p)/M)\omega_p$. In this study, we assumed that the SBP has the same ω_{\max} and the same number of harmonic oscillators M as the other heat baths.

The time-dependent population of site n can be obtained according to⁵⁸

$$\langle \hat{P}_{nn}(t) \rangle = \sum_{\beta\beta'} \int d\mathbf{X}(0) \mathcal{P}_{nn}^{\beta\beta'}(t) \rho_N^{\beta'\beta}(0) \rho_{E,W}(0) \quad (17)$$

The initial distribution of the environment is $\rho_{E,W}(0) = \rho_{B,W}(0)$ if $\chi = 0$ and $\rho_{E,W}(0) = \rho_{B,W}(0)\rho_{P,W}(0)$ if $\chi = 1$. Here

$$\rho_{B,W}(0) = \prod_{n=1,4} \prod_{j=1}^M \frac{\tanh(\beta\omega_{n,j}/2)}{\pi} \times \exp\left[-\frac{2 \tanh(\beta\omega_{n,j}/2)}{\omega_{n,j}} \left(\frac{P_{n,j}^2}{2} + \frac{\omega_{n,j}^2 R_{n,j}^2}{2}\right)\right]$$

and an analogous expression for $\rho_{P,W}(0)$ are the partially Wigner-transformed thermal equilibrium states for the baths and the SBP, respectively.⁵⁹ Since $\rho_{E,W}(0)$ is a normalized distribution function for the environments' coordinates, we can perform trajectory-based molecular dynamics simulations to compute the time-dependent site populations in eq 17 as follows: We generate a swarm of independent classical-like trajectories starting from different $\mathbf{X}(0)$ sampled from the partially Wigner-transformed environmental initial distribution $\rho_{E,W}(0)$ and the same initial values of the matrix elements $\mathcal{P}_{nm}^{\beta\beta'}$ (viz., $\mathcal{P}_{nn}^{\beta\beta'}(0) = 1$ and the initial values of the remaining matrix elements are zero). Each trajectory of $\mathcal{P}_{nm}^{\beta\beta'}(t)$ is obtained by integrating eq 14 using the standard fourth-order Runge-Kutta method.⁶⁰ Finally, we average $\mathcal{P}_{nm}^{\beta\beta'}(t)$ over the ensemble of trajectories, taking into account the weight $\rho_N^{\beta'\beta}(0)$ (determined by the initial state of the network $\hat{\rho}_N(0)$), and then sums over the indices $\beta\beta'$ to obtain $\langle \hat{P}_{nn}(t) \rangle$ for site n .

4. RESULTS AND DISCUSSION

4.1. Demonstration of the Working Principle: Storage and Discharge. As the loss-free character of the proposed EQB is independent of parameters (see eq 12), for demonstration purposes, we choose the following parameters: $E_1 = 250 \text{ cm}^{-1}$, $E_{i \in \{2,3,5,6\}} = 200 \text{ cm}^{-1}$, $E_4 = 0 \text{ cm}^{-1}$, and $h = -60 \text{ cm}^{-1}$. The energy gaps between the SSs and BSs establish energy barriers to direct the flow of population toward the exit site (i.e., site 4)

when discharging the EQB (cf. the bias voltage in traditional lithium-ion batteries, for example).

The simulated time-dependent site populations of the OQN in the storage ($\chi = 0$) and discharging ($\chi = 1$) phases are shown in Figure 1. From Figure 1a, it is evident that the site populations are indeed time-independent in the absence of the SBP, even though the SSs are coupled to thermal baths. Populations take values according to eq 12, implying that the electronic excitation energy can be completely stored within the bulk states of the EQB for an arbitrary long time. In other words, the EQB is loss free. To harness the stored excitation energy, we attach a symmetry-breaking reservoir, which nonlocally acts on sites 2 and 3 of the OQN. This element breaks the exchange symmetry and thus allows us to populate the exit site 4. As can be seen from Figure 1b, the populations of all sites now vary with time. The populations of the BSs decrease as a function of time, whereas the population of site 4 increases (the population of site 1 first increases, and then it saturates due to the energy structure of the network, which directs the excitation energy flow toward site 4). Thus, DECIDE, although an approximate method, is capable of reproducing the exact result without the SBP and it (at least) qualitatively reproduces the expected trends when the SBP is enacted.

The energy gap between the two SSs (1 and 4) mimics the bias voltage in traditional chemical batteries. We therefore expect that a larger energy gap will be advantageous in enhancing the performance of the EQB. To explore this possibility, we take $E_1 = 400 \text{ cm}^{-1}$ instead of $E_1 = 250 \text{ cm}^{-1}$, with the other site energies fixed. The resulting time-dependent site populations of the OQN, with and without the SBP, are depicted in Figure 2. First, in panel (a), we confirm that the population dynamics during the storage phase is independent of the parameters we choose, since the exchange symmetry is preserved. As for the

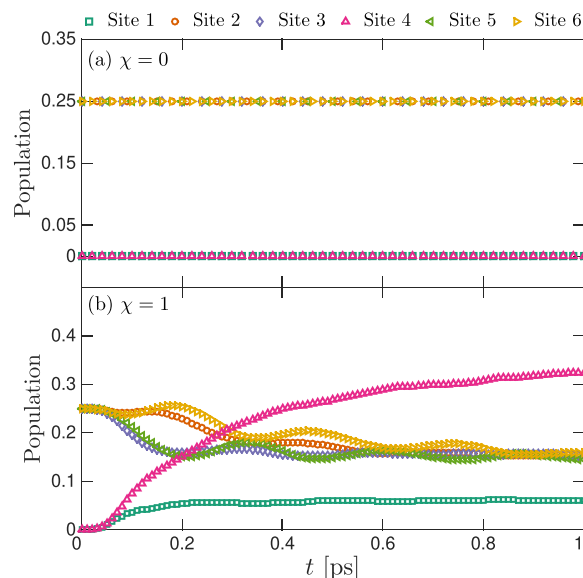


Figure 2. Time-dependent site populations for the OQN during storage (a) and discharge (b) under a larger bias of $E_1 = 400 \text{ cm}^{-1}$, instead of the choice of $E_1 = 250 \text{ cm}^{-1}$. Results for sites 1, 2, 3, 4, 5, and 6 are represented by squares, circles, diamonds, upward-pointing triangles, left-pointing triangles, and right-pointing triangles, respectively. A time step of $\Delta t = 1 \text{ fs}$ and an ensemble of 1×10^4 trajectories are used to obtain converged DECIDE results. The other parameters are the same as those in Figure 1.

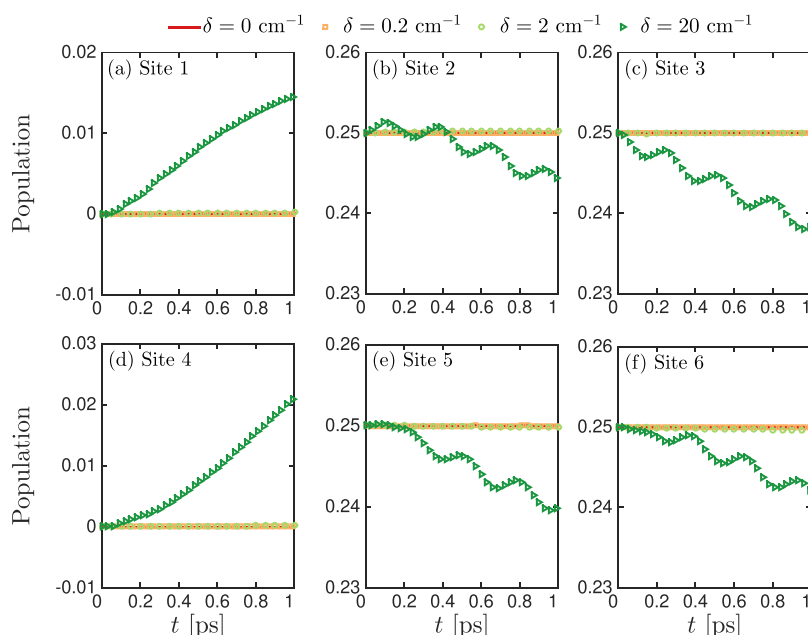


Figure 3. Role of diagonal disorder on the storage stage of the EQB. (a–f) Time-dependent populations of the six sites for the OQN without an SBP under various diagonal disorder widths, $\delta = 0 \text{ cm}^{-1}$ (solid), $\delta = 0.2 \text{ cm}^{-1}$ (square), $\delta = 2 \text{ cm}^{-1}$ (circle), and $\delta = 20 \text{ cm}^{-1}$ (triangle). An average over 1000 uniformly distributed random disorders is performed to achieve convergence (error bars are much smaller than the symbols). For each sample, a time step of $\Delta t = 1 \text{ fs}$ and an ensemble of 1×10^4 trajectories are used to obtain converged DECIDE results. Parameters are the same as those in Figure 1a.

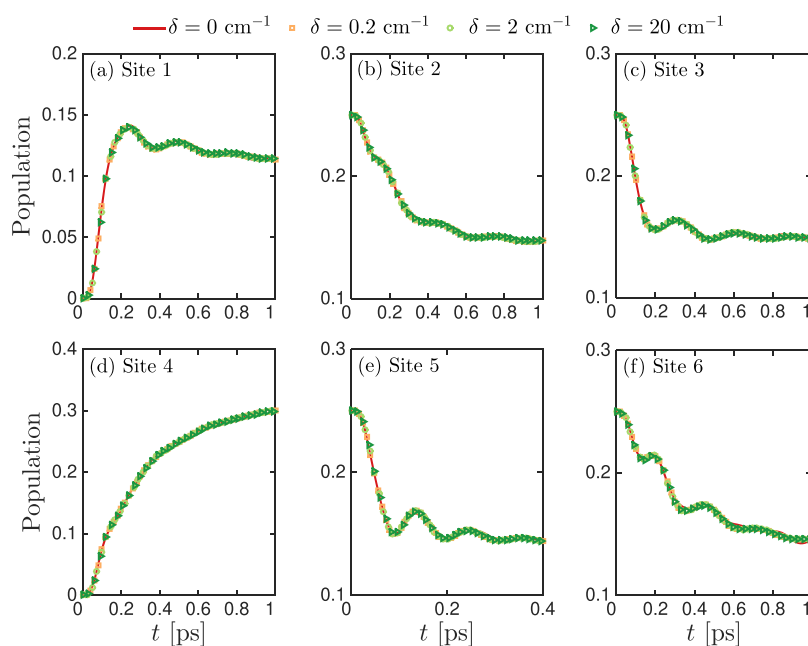


Figure 4. Role of diagonal disorder on the discharge stage of the EQB. (a–f) Time-dependent populations of the six sites for the OQN with the SBP acting on sites 2 and 3 under various diagonal disorder widths, $\delta = 0 \text{ cm}^{-1}$ (solid), $\delta = 0.2 \text{ cm}^{-1}$ (square), $\delta = 2 \text{ cm}^{-1}$ (circle), and $\delta = 20 \text{ cm}^{-1}$ (triangle). An average over 1000 uniformly distributed random disorders is performed to achieve convergence (error bars are much smaller than the symbols). For each sample, a time step of $\Delta t = 1 \text{ fs}$ and an ensemble of 1×10^4 trajectories are used to obtain converged DECIDE results. The parameters are the same as those in Figure 1b.

discharge phase, comparing Figure 2b with Figure 1b, we find that for the larger bias, the population accumulating in time at site 1 is indeed largely suppressed, whereas more population can be extracted from the bulk and directed toward the exit site 4. Although here we only consider two sets of parameters, we should emphasize that similar conclusions can be reached with other choices of parameters. Together, the results in Figures 1

and 2 demonstrate the underlying working principles of the EQB and highlight its potential functionality.

How general and flexible is the proposed EQB? The actual values of the parameters E_1 , $E_{B,S}$, E_4 , and h are in fact arbitrary, as any choice would satisfy the symmetry requirements of the EQB. Moreover, the intersite coupling h does not need to be uniform; the setup operates under reduced symmetry as long as it satisfies $J_{1,2} = J_{1,6}$, $J_{3,4} = J_{4,5}$, and $J_{2,3} = J_{5,6}$. Realizations of the EQB are

possible with engineered devices for which an appropriate model Hamiltonian can be devised³⁵ and whose environments may be controlled. However, even in such cases, achieving perfect structural symmetry is highly unlikely due to experimental limitations and static/dynamic disorder. In the following subsections, we therefore assess the impact of energy disorder (diagonal and off-diagonal), as well as temperature fluctuations of the SBP.

4.2. Effects of Diagonal Disorder. We consider the effect of static diagonal disorder on the OQN by shifting the energy of each site, E_n , by ΔE_n , which is randomly chosen from a uniform distribution of width δ , i.e., $\Delta E_n \in \left[-\frac{\delta}{2}, \frac{\delta}{2}\right]$. The corresponding EET properties are calculated by averaging over 1000 realizations of the disorder, with each sample requiring 1×10^4 trajectories to obtain converged DECIDE results. Results for the site populations, during storage and discharge, for different values of δ are shown in Figures 3 and 4, respectively.

First, we examine the role of static diagonal disorder on the storage phase in Figure 3. We observe that as long as the disorder is weak (viz., $\delta = 0.2, 2 \text{ cm}^{-1}$), it does not degrade the excitation energy storage performance, underscoring the robustness of the proposed EQB. Only once we increase the width δ to 20 cm^{-1} , which corresponds to a strong diagonal disorder (recall that the energy of the bulk sites is 200 cm^{-1}), are the structural symmetry and associated exchange symmetry non-negligibly broken. Consequently, we observe energy leakage from the BSs (2, 3, 5, 6) while the SSs (1, 4) gain population in time, rendering the OQN unsuitable for long-term excitation energy storage. Nevertheless, we point out that the magnitude of population loss is only of the order of 10^{-2} within the considered time window.

Next, in Figure 4, we study the role of static diagonal disorder during the discharge stage, with the SBP attached. Here, even a strong disorder only leads to a minor impact on the population dynamics. Therefore, diagonal disorder does not strongly affect the performance of the EQB during the discharging phase, although strong disorder during the storage phase makes the EQB unstable. We attribute this difference to the fact that the SBP completely breaks the structural symmetry, thereby making the EQB less sensitive to diagonal disorder.

To complement the simulations of the population dynamics under various degrees of static diagonal disorder, we calculate the transfer efficiency, defined in eq 7, as a way of assessing the impact of diagonal disorder on the efficiency of the excitation energy transfer to the sink of the EQB. In Figure 5, we show results for the transfer efficiency of the EQB with ($\chi = 1$) and without ($\chi = 0$) the SBP under various levels of diagonal disorder. In a perfectly symmetric OQN without the SBP, the transfer efficiency is identically zero, implying that the energy is stored in the bulk and cannot be harnessed through the exit site. Only a strong diagonal disorder (20 cm^{-1}) can induce nonzero transfer efficiency in the absence of the SBP. In contrast, in the symmetry-broken OQN ($\chi = 1$), the transfer efficiency remains almost the same under different degrees of diagonal disorder. It should be noted that our total simulation time for obtaining the transfer efficiency is limited to a value for which $\eta(t) \ll 1$, to ensure the validity of the definition of the time-dependent transfer efficiency in eq 7. This is because our equations of motion for the subsystem do not contain a non-Hermitian term responsible for exciton trapping from the exit site to the sink.

4.3. Effects of Off-Diagonal Disorder. We now investigate the effect of static off-diagonal disorder, which mimics the

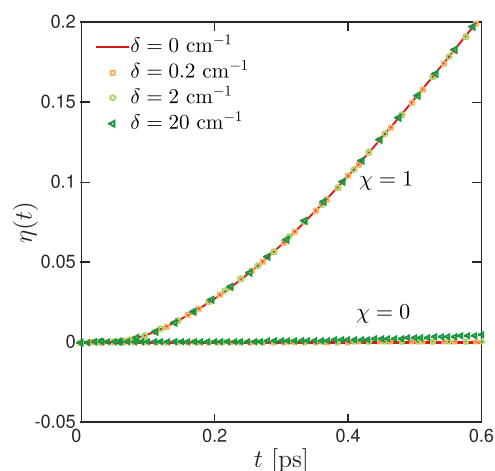


Figure 5. Time-dependent transfer efficiency, $\eta(t)$, for OQNs without an SBP ($\chi = 0$) and with an SBP acting on sites 2 and 3 ($\chi = 1$) for various diagonal disorder widths $\delta = 0 \text{ cm}^{-1}$ (solid), $\delta = 0.2 \text{ cm}^{-1}$ (square), $\delta = 2 \text{ cm}^{-1}$ (circle), and $\delta = 20 \text{ cm}^{-1}$ (triangle). An average over 1000 uniformly distributed random disorders is performed to achieve convergence (error bars are much smaller than the symbols). For each sample, a time step of $\Delta t = 1 \text{ fs}$ and an ensemble of 1×10^4 trajectories are used to obtain converged DECIDE results. The bath and SBP parameters are the same as in Figure 1.

fluctuations in the excitonic coupling strength due to non-Condon effects. This is accomplished by adding to the nearest-neighbor electronic coupling strength, h , a contribution ΔV_{nm} , which is randomly chosen from a uniform distribution of width σ , i.e., $\Delta V_{nm} \in \left[-\frac{\sigma}{2}, \frac{\sigma}{2}\right]$. Also, to pinpoint the effects of off-diagonal disorder, the site energies are held fixed. The corresponding EET properties are calculated by averaging over 1000 configurations of the disorder, with each sample requiring 1×10^4 trajectories to obtain converged DECIDE results. The results for the time-dependent site populations, with and without the SBP, for different values of σ are displayed in Figures 6 and 7, respectively.

During the storage phase, we observe in Figure 6 that under a very weak off-diagonal disorder ($\sigma = 0.1 \text{ cm}^{-1}$), the EQB is essentially loss free. The populations of the BSs only begin to deviate from their optimal values of 0.25 for an intermediate degree of disorder, viz., $\sigma = 1 \text{ cm}^{-1}$. Interestingly, however, if we further increase the width of the off-diagonal disorder by an order of magnitude to $\sigma = 10 \text{ cm}^{-1}$, there is no significant additional degradation in the performance of the EQB. Only a very small amount of the stored energy is leaked out of the bulk of the EQB. Contrasting this with the diagonal disorder case in Figure 3, we observe here two distinct differences: (i) The populations of the BSs do not follow a specific trend; some sites gain population, whereas others lose population (at least for the time period considered), implying that the EQB prefers to redistribute the stored excitonic energy among the BSs rather than leak it to the SSs, even in the presence of strong off-diagonal disorder. (Note that $\sigma = 10 \text{ cm}^{-1}$ is of the same order of magnitude as the bare electronic coupling strength h .) (ii) The overall effect of the off-diagonal disorder is significantly smaller than that of the diagonal disorder. Even with a strong off-diagonal disorder, e.g., $\sigma = 10 \text{ cm}^{-1}$, the deviation from the ideal EQB storage value is only on the order of 10^{-4} . This difference can also be observed by comparing the efficiency result in Figure 8 with that in Figure 5.

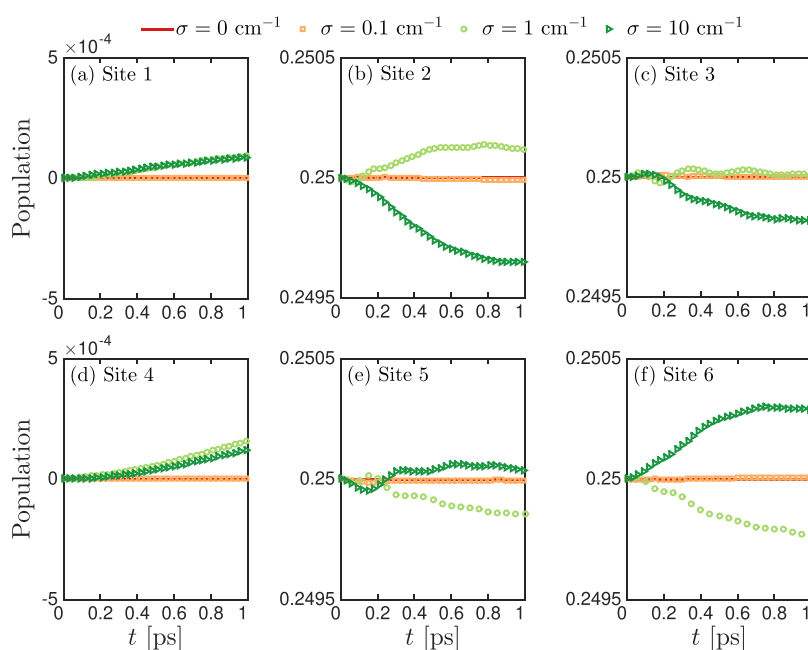


Figure 6. Role of off-diagonal disorder on the storage stage of the EQB. (a–f) Time-dependent populations of the six sites for the OQN without an SBP under various off-diagonal disorder widths, $\sigma = 0 \text{ cm}^{-1}$ (solid), $\sigma = 0.1 \text{ cm}^{-1}$ (square), $\sigma = 1 \text{ cm}^{-1}$ (circle), and $\sigma = 10 \text{ cm}^{-1}$ (triangle). An average over 1000 uniformly distributed random disorders is performed to achieve convergence (error bars are much smaller than the symbols). For each sample, a time step of $\Delta t = 1 \text{ fs}$ and an ensemble of 1×10^4 trajectories are used to obtain converged DECIDE results. Parameters are the same as in Figure 1a.

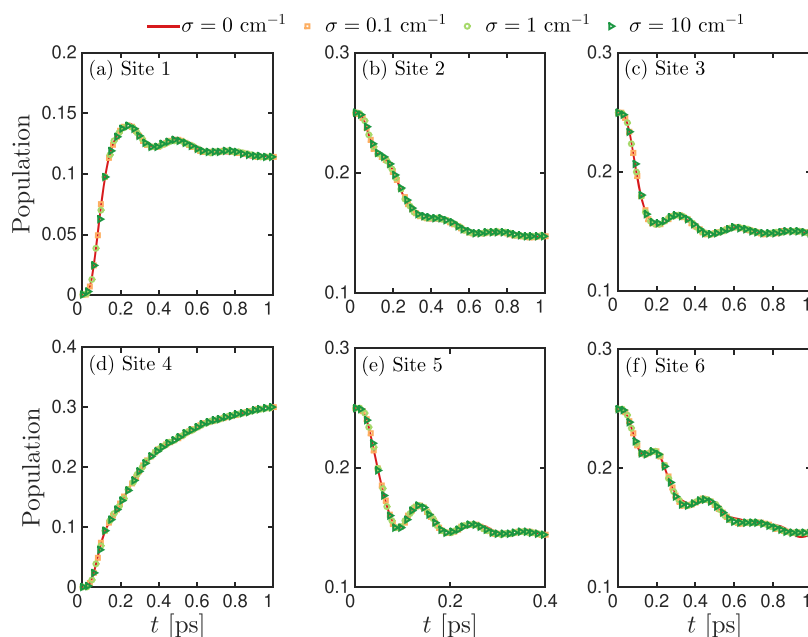


Figure 7. Role of off-diagonal disorder in the discharge stage of the EQB. (a–f) Time-dependent populations of the six sites for the OQN with the SBP acting on sites 2 and 3 under various off-diagonal disorder widths, $\sigma = 0 \text{ cm}^{-1}$ (solid lines), $\sigma = 0.1 \text{ cm}^{-1}$ (square), $\sigma = 1 \text{ cm}^{-1}$ (circle), and $\sigma = 10 \text{ cm}^{-1}$ (triangle). An average over 1000 uniformly distributed random disorders is performed to achieve convergence (error bars are much smaller than the symbols). For each sample, a time step of $\Delta t = 1 \text{ fs}$ and an ensemble of 1×10^4 trajectories are used to obtain converged DECIDE results. Parameters are the same as those in Figure 1b.

We next turn to the EQB in its discharging stage. As can be seen from Figure 7, the site populations are negligibly affected by the static off-diagonal disorder. Together, Figures 4 and 7 reveal that the proposed EQB is quite insensitive to structural fluctuations when an SBP is attached and can maintain its optimal efficiency during the discharging process in the presence of strong static disorder, whether diagonal or off-diagonal. This

can also be observed by comparing the efficiency result in Figure 8 with that in Figure 5.

4.4. Effects of SBP Temperature. From an experimental point of view, the SBP (which is realized here by attaching a heat bath) may only contain a finite number of degrees of freedom and hence its temperature may fluctuate and deviate from that of the two attached heat baths. To maintain the functionality of the

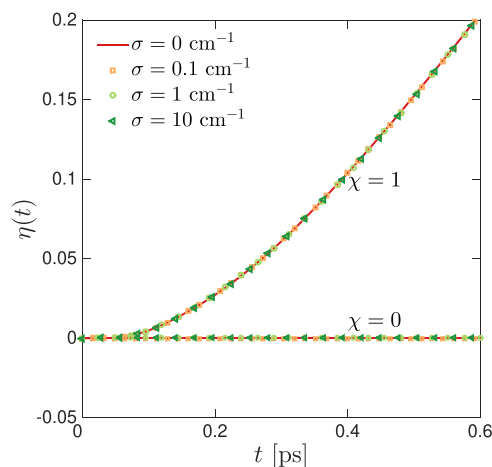


Figure 8. Time-dependent transfer efficiency, $\eta(t)$, for OQNs without a SBP ($\chi = 0$) and with a SBP acting on sites 2 and 3 ($\chi = 1$) for various off-diagonal disorder widths, $\sigma = 0 \text{ cm}^{-1}$ (solid), $\sigma = 0.1 \text{ cm}^{-1}$ (square), $\sigma = 1 \text{ cm}^{-1}$ (circle), and $\sigma = 10 \text{ cm}^{-1}$ (triangle). An average over 1000 uniformly distributed random disorders is performed to achieve convergence (error bars are much smaller than the symbols). For each sample, a time step of $\Delta t = 1 \text{ fs}$ and an ensemble of 1×10^4 trajectories are used to obtain converged DECIDE results. The bath and SBP parameters are the same as those in Figure 1.

EQB, it is desirable that the SBP does not significantly alter the population dynamics of the network in the presence of a small temperature difference. To check whether our setup satisfies this criterion, we vary the temperature T_p of the SBP to create a small temperature gradient between the OQN and SBP and study the resulting EET properties. Comparisons between the time-dependent site populations for different temperatures of the SBP are shown in Figure 9. As can be seen, the population dynamics remains almost the same regardless of the temperature difference between the SBP and OQN. A comparison of the

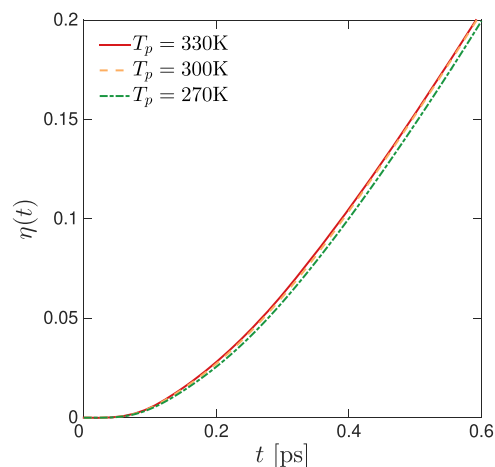


Figure 10. Time-dependent transfer efficiency, $\eta(t)$, for different temperatures of the SBP, $T_p = 330 \text{ K}$ (solid), $T_p = 300 \text{ K}$ (dashed), and $T_p = 270 \text{ K}$ (dash-dotted). A time step of $\Delta t = 1 \text{ fs}$ and an ensemble of 1×10^4 trajectories are used to obtain converged DECIDE results. The other parameters are the same as in Figure 1b.

transfer efficiency of the EQB for different T_p 's is shown in Figure 10. It is clear that the transfer efficiency of the EQB is essentially independent of the temperature of the SBP reservoir. These results confirm the role of this attached bath as a symmetry-breaking perturbation to the dynamics of the OQN.

5. SUMMARY

In this paper, we tackled the challenge of achieving long-term energy storage in quantum batteries subject to environmental effects. Resorting to an open quantum system setup, we proposed an excitonic quantum battery that is loss-free during its storage phase. This was made possible by preparing the quantum battery in a symmetry-protected dark state living in a decoherence-free subspace. Due to the passive symmetry

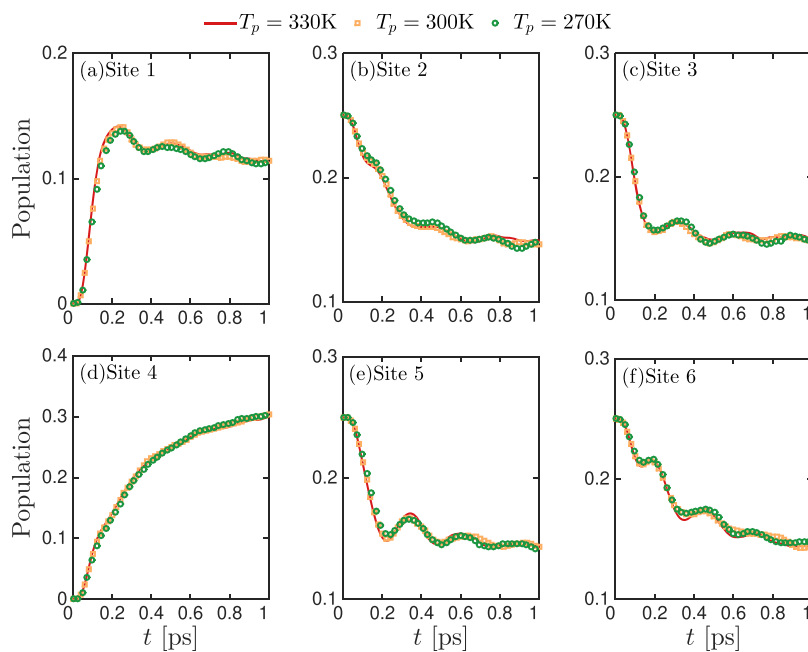


Figure 9. (a–f) Time-dependent populations of the six sites for the OQN with the SBP acting on sites 2 and 3 for different SBP temperatures, $T_p = 330 \text{ K}$ (solid), $T_p = 300 \text{ K}$ (square), and $T_p = 270 \text{ K}$ (circle). A time step of $\Delta t = 1 \text{ fs}$ and an ensemble of 1×10^4 trajectories are used to obtain converged DECIDE results. The other parameters are the same as in Figure 1b.

protection, the excitonic energy can be stored for long times even in the presence of thermal environments that may substantially couple to the OQN, a highly desirable feature for energy storage applications. The EQB is discharged by attaching to it a symmetry-breaking perturbation, here in the form of a thermal reservoir, which destroys the dark state.

To illustrate the potential functionality and working mechanism of the proposed EQB, we studied an OQN with a *para*-benzene-like structure, for which one can easily construct an exchange symmetry operator and symmetry-protected dark states. Numerical results for this model, generated using the recently developed DECIDE method, demonstrated the possibility of realizing a loss-free EQB. We also investigated the effects of diagonal and off-diagonal disorders on the storage and discharge phases of the EQB and the effect of varying the SBP temperature on the discharging process. Our simulation results showed that the proposed EQB is rather robust against perturbations to the structural symmetry.

Before concluding, it is worth commenting on a related research endeavor to understand the role of molecular structure and symmetry on the electrical conductance of molecules (see refs 53, 61–66, for example). Specifically, constructive and destructive interference effects, emerging from interfering electron pathways, were examined in refs 53, 61–66 to devise nontrivial molecular-based circuits. Although the majority of studies in the area of molecular electronics consider a steady-state behavior and ignore decoherence effects, ref 53 focused on the time-dependent electrical currents in *para*- and *meta*-substituted benzene molecules under the influence of decoherence. In this study, it was demonstrated that in the absence of decoherence, *para*-substituted benzene supports high currents whereas *meta*-substituted benzene suffers from a destructive interference effect and essentially acts as an insulator. However, once decoherence is included (using a probe), the interference pattern is disrupted and conductance is restored in *meta*-substituted benzene. This behavior parallels our exploitation of the benzene molecule symmetry to store the excitonic energy and our use of a symmetry-breaking perturbation to release it.

Although we have not attempted to maximize the transfer efficiency of the EQB, this can, in principle, be done by exploring the parameter space and identifying optimal parameter sets. Extensions to this work could include applying the working principles to more complicated networks, such as those encountered in artificial light-harvesting complexes,^{67–69} modeling open charged EQBs by means of Lindblad master equations with symmetries,^{42,48–50,70} investigating ways of initializing the EQB in a dark state, and optimizing the charging/discharging processes.

AUTHOR INFORMATION

Corresponding Authors

*E-mail: junj.liu@utoronto.ca (J.L.).

*E-mail: gabriel.hanna@ualberta.ca (G.H.).

ORCID

Junjie Liu: 0000-0002-9963-9052

Dvira Segal: 0000-0002-8027-8920

Gabriel Hanna: 0000-0003-0554-8887

Notes

The authors declare no competing financial interest.

ACKNOWLEDGMENTS

J.L. and G.H. acknowledge support from the Natural Sciences and Engineering Research Council of Canada (NSERC). D.S. acknowledges support from an NSERC Discovery Grant and the Canada Research Chair program.

REFERENCES

- (1) Lewis, N. S. Toward Cost-Effective Solar Energy Use. *Science* **2007**, *315*, 798–801.
- (2) Cook, T. R.; Dogutan, D. K.; Reece, S. Y.; Surendranath, Y.; Teets, T. S.; Nocera, D. G. Solar Energy Supply and Storage for the Legacy and Nonlegacy Worlds. *Chem. Rev.* **2010**, *110*, 6474–6502.
- (3) Kucharski, T. J.; Tian, Y.; Akbulatov, S.; Boulatov, R. Chemical Solutions for the Closed-Cycle Storage of Solar Energy. *Energy Environ. Sci.* **2011**, *4*, 4449–4472.
- (4) Pitié, F.; Zhao, C.; Cáceres, G. Thermo-mechanical Analysis of Ceramic Encapsulated Phase-Change-Material (PCM) Particles. *Energy Environ. Sci.* **2011**, *4*, 2117–2124.
- (5) Alicki, R.; Fannes, M. Entanglement Boost for Extractable Work from Ensembles of Quantum Batteries. *Phys. Rev. E* **2013**, *87*, No. 042123.
- (6) Hovhannisyan, K. V.; Perarnau-Llobet, M.; Huber, M.; Acín, A. Entanglement Generation is Not Necessary for Optimal Work Extraction. *Phys. Rev. Lett.* **2013**, *111*, No. 240401.
- (7) Binder, F. C.; Vinjanampathy, S.; Modi, K.; Goold, J. Quantacell: Powerful Charging of Quantum Batteries. *New J. Phys.* **2015**, *17*, No. 075015.
- (8) Campaioli, F.; Pollock, F. A.; Binder, F. C.; Céleri, L.; Goold, J.; Vinjanampathy, S.; Modi, K. Enhancing the Charging Power of Quantum Batteries. *Phys. Rev. Lett.* **2017**, *118*, No. 150601.
- (9) Ferraro, D.; Campisi, M.; Andolina, G. M.; Pellegrini, V.; Polini, M. High-Power Collective Charging of a Solid-State Quantum Battery. *Phys. Rev. Lett.* **2018**, *120*, No. 117702.
- (10) Le, T. P.; Levinsen, J.; Modi, K.; Parish, M. M.; Pollock, F. A. Spin-chain Model of a Many-Body Quantum Battery. *Phys. Rev. A* **2018**, *97*, No. 022106.
- (11) Tserkovnyak, Y.; Xiao, J. Energy Storage via Topological Spin Textures. *Phys. Rev. Lett.* **2018**, *121*, No. 127701.
- (12) Andolina, G. M.; Farina, D.; Mari, A.; Pellegrini, V.; Giovannetti, V.; Polini, M. Charger-Mediated Energy Transfer in Exactly-Solvable Models for Quantum Batteries. *Phys. Rev. B* **2018**, *98*, No. 205423.
- (13) Andolina, G. M.; Keck, M.; Mari, A.; Campisi, M.; Polini, V. G. M. Extractable Work, the Role of Correlations, and Asymptotic Freedom in Quantum Batteries. *Phys. Rev. Lett.* **2019**, *122*, No. 047702.
- (14) Farina, D.; Andolina, G. M.; Mari, A.; Polini, M.; Giovannetti, V. Charger-Mediated Energy Transfer for Quantum Batteries: An Open System Approach. *Phys. Rev. B* **2019**, *99*, No. 035421.
- (15) Julià-Farré, S.; Salamon, T.; Riera, A.; Bera, M. N.; Lewenstein, M. Bounds on Capacity and Power of Quantum Batteries. 2018, arXiv:1811.04005. arXiv.org e-Print archive. <https://arxiv.org/abs/1811.04005>.
- (16) Campaioli, F.; Pollock, F. A.; Vinjanampathy, S. In *Thermodynamics in the Quantum Regime: Recent Progress and Outlook*; Binder, F., Correa, L. A., Gogolin, C., Anders, J., Adesso, G., Eds.; Springer, 2018.
- (17) Andolina, G. M.; Keck, M.; Mari, A.; Campisi, M.; Polini, V. G. M. Quantum versus Classical Many-Body Batteries. *Phys. Rev. B* **2019**, *99*, No. 205437.
- (18) Breuer, H.-P.; Petruccione, F. *The Theory of Open Quantum Systems*; Oxford University Press: Oxford, 2006.
- (19) Weiss, U. *Quantum Dissipative Systems*; World Scientific: Singapore, 2012.
- (20) de Vega, I.; Alonso, D. Dynamics of Non-Markovian Open Quantum Systems. *Rev. Mod. Phys.* **2017**, *89*, No. 015001.
- (21) Barra, F. Dissipative Charging of a Quantum Battery. *Phys. Rev. Lett.* **2019**, *122*, No. 210601.
- (22) Suter, D.; Álvarez, G. A. Colloquium: Protecting Quantum Information against Environmental Noise. *Rev. Mod. Phys.* **2016**, *88*, No. 041001.

- (23) Zanardi, P.; Rasetti, M. Noiseless Quantum Codes. *Phys. Rev. Lett.* **1997**, *79*, 3306–3309.
- (24) Lidar, D. A.; Chuang, I. L.; Whaley, K. B. Decoherence-Free Subspaces for Quantum Computation. *Phys. Rev. Lett.* **1998**, *81*, 2594–2597.
- (25) Kielpinski, D.; Meyer, V.; Rowe, M. A.; Sackett, C. A.; Itano, W. M.; Monroe, C.; Wineland, D. J. A Decoherence-Free Quantum Memory Using Trapped Ions. *Science* **2001**, *291*, 1013–1015.
- (26) Lidar, D. A.; Birgitta Whaley, K. In *Irreversible Quantum Dynamics*; Benatti, F., Floreanini, R., Eds.; Springer: Berlin, Heidelberg, 2003; pp 83–120.
- (27) Qin, W.; Wang, C.; Zhang, X. Protected Quantum-state Transfer in Decoherence-Free Subspaces. *Phys. Rev. A* **2015**, *91*, No. 042303.
- (28) Zhao, P. Z.; Xu, G. F.; Ding, Q. M.; Sjöqvist, E.; Tong, D. M. Single-shot Realization of Nonadiabatic Holonomic Quantum Gates in Decoherence-Free Subspaces. *Phys. Rev. A* **2017**, *95*, No. 062310.
- (29) Kockum, A. F.; Johansson, G.; Nori, F. Decoherence-Free Interaction between Giant Atoms in Waveguide Quantum Electrodynamics. *Phys. Rev. Lett.* **2018**, *120*, No. 140404.
- (30) Chin, A. W.; Datta, A.; Caruso, F.; Huelga, S. F.; Plenio, M. B. Noise-Assisted Energy Transfer in Quantum Networks and Light-Harvesting Complexes. *New J. Phys.* **2010**, *12*, No. 065002.
- (31) Scholak, T.; de Melo, F.; Wellens, T.; Mintert, F.; Buchleitner, A. Efficient and Coherent Excitation Transfer Across Disordered Molecular Networks. *Phys. Rev. E* **2011**, *83*, No. 021912.
- (32) Walschaers, M.; Diaz, J. F.-d.-C.; Mulet, R.; Buchleitner, A. Optimally Designed Quantum Transport across Disordered Networks. *Phys. Rev. Lett.* **2013**, *111*, No. 180601.
- (33) Walschaers, M.; Mulet, R.; Wellens, T.; Buchleitner, A. Statistical Theory of Designed Quantum Transport Across Disordered Networks. *Phys. Rev. E* **2015**, *91*, No. 042137.
- (34) Baker, L. A.; Habershon, S. Robustness, Efficiency, and Optimality in the Fenna-Matthews-Olson Photosynthetic Pigment-Protein Complex. *J. Chem. Phys.* **2015**, *143*, No. 105101.
- (35) Santos, A. C.; Cakmak, B.; Campbell, S.; Zinner, N. T. Stable Adiabatic Quantum Batteries. 2019, arXiv:1906.01364. arXiv.org e-Print archive. <https://arxiv.org/abs/1906.01364>.
- (36) Vitanov, N. V.; Rangelov, A. A.; Shore, B. W.; Bergmann, K. Stimulated Raman Adiabatic Passage in Physics, Chemistry, and Beyond. *Rev. Mod. Phys.* **2017**, *89*, No. 015006.
- (37) Frenkel, J. On the Transformation of Light into Heat in Solids. I. *Phys. Rev.* **1931**, *37*, 17–44.
- (38) Davydov, A. S. *Theory of Molecular Excitons*; Plenum Press: New York, London, 1971.
- (39) May, V.; Kühn, O. *Charge and Energy Transfer Dynamics in Molecular Systems*; Wiley-VCH: Weinheim, 2011.
- (40) Reibtrost, P.; Mohseni, M.; Kassal, I.; Lloyd, S.; Aspuru-Guzik, A. Environment-Assisted Quantum Transport. *New J. Phys.* **2009**, *11*, No. 033003.
- (41) Ishizaki, A.; Fleming, G. R. Theoretical Examination of Quantum Coherence in a Photosynthetic System at Physiological Temperature. *Proc. Natl. Acad. Sci. U.S.A.* **2009**, *106*, 17255–17260.
- (42) Thingna, J.; Manzano, D.; Cao, J. Dynamical Signatures of Molecular Symmetries in Nonequilibrium Quantum Transport. *Sci. Rep.* **2016**, *6*, No. 28027.
- (43) Beige, A.; Braun, D.; Tregenna, B.; Knight, P. L. Quantum Computing Using Dissipation to Remain in a Decoherence-Free Subspace. *Phys. Rev. Lett.* **2000**, *85*, 1762–1765.
- (44) Xue, P.; Xiao, Y.-F. Universal Quantum Computation in Decoherence-Free Subspace with Neutral Atoms. *Phys. Rev. Lett.* **2006**, *97*, No. 140501.
- (45) Kraus, B.; Büchler, H. P.; Diehl, S.; Kantian, A.; Micheli, A.; Zoller, P. Preparation of Entangled States by Quantum Markov Processes. *Phys. Rev. A* **2008**, *78*, No. 042307.
- (46) Diehl, S.; Micheli, A.; Kantian, A.; Kraus, B.; Büchler, H. P.; Zoller, P. Quantum States and Phases in Driven Open Quantum Systems with Cold Atoms. *Nat. Phys.* **2008**, *4*, 878–883.
- (47) Verstraete, F.; Wolf, M. M.; Cirac, J. I. Quantum Computation, Quantum State Engineering, and Quantum Phase Transitions Driven by Dissipation. *Nat. Phys.* **2009**, *5*, 633–636.
- (48) Buča, B.; Prosen, T. A Note on Symmetry Reductions of the Lindblad Equation: Transport in Constrained Open Spin Chains. *New J. Phys.* **2012**, *14*, No. 073007.
- (49) Albert, V. V.; Jiang, L. Symmetries and Conserved Quantities in Lindblad Master Equations. *Phys. Rev. A* **2014**, *89*, No. 022118.
- (50) Manzano, D.; Hurtado, P. Harnessing Symmetry to Control Quantum Transport. *Adv. Phys.* **2018**, *67*, 1–67.
- (51) Allegra, M.; Giorda, P.; Lloyd, S. Global Coherence of Quantum Evolutions based on Decoherent Histories: Theory and Application to Photosynthetic Quantum Energy Transport. *Phys. Rev. A* **2016**, *93*, No. 042312.
- (52) Mohseni, M.; Reibtrost, P.; Lloyd, S.; Aspuru-Guzik, A. Environment-Assisted Quantum Walks in Photosynthetic Energy Transfer. *J. Chem. Phys.* **2008**, *129*, No. 174106.
- (53) Chen, S.; Zhang, Y.; Koo, S.; Tian, H.; Yam, C.; Chen, G.; Ratner, M. A. Interference and Molecular Transport—A Dynamical View: Time-Dependent Analysis of Disubstituted Benzenes. *J. Phys. Chem. Lett.* **2014**, *5*, 2748–2752.
- (54) Liu, J.; Hanna, G. Efficient and Deterministic Propagation of Mixed Quantum-Classical Liouville Dynamics. *J. Phys. Chem. Lett.* **2018**, *9*, 3928–3933.
- (55) Wigner, E. On the Quantum Correction For Thermodynamic Equilibrium. *Phys. Rev.* **1932**, *40*, 749.
- (56) Kapral, R.; Ciccotti, G. Mixed Quantum-Classical Dynamics. *J. Chem. Phys.* **1999**, *110*, 8919–8929.
- (57) Wang, H.; Thoss, M.; Miller, W. H. Systematic Convergence in the Dynamical Hybrid Approach for Complex Systems: A Numerically Exact Methodology. *J. Chem. Phys.* **2001**, *115*, 2979–2990.
- (58) Sergi, A.; MacKernan, D.; Ciccotti, G.; Kapral, R. Simulating Quantum Dynamics in Classical Environments. *Theor. Chem. Acc.* **2003**, *110*, 49–58.
- (59) Imre, K.; Özizmir, E.; Rosenbaum, M.; Zweifel, P. F. Wigner Method in Quantum Statistical Mechanics. *J. Math. Phys.* **1967**, *8*, 1097–1108.
- (60) Dormand, J. R.; Prince, P. J. A Family of Embedded Runge-Kutta Formulae. *J. Comput. Appl. Math.* **1980**, *6*, 19–26.
- (61) Solomon, G. C.; Andrews, D. Q.; Hansen, T.; Goldsmith, R. H.; Wasielewski, M. R.; Dwyne, R. P. V.; Ratner, M. A. Understanding Quantum Interference in Coherent Molecular Conduction. *J. Chem. Phys.* **2008**, *129*, No. 054701.
- (62) Hansen, T.; Solomon, G. C.; Andrews, D. Q.; Ratner, M. A. Interfering Pathways in Benzene: An Analytical Treatment. *J. Chem. Phys.* **2009**, *131*, No. 194704.
- (63) Nozaki, D.; Toher, C. Is the Antiresonance in Meta-Contacted Benzene Due to the Destructive Superposition of Waves Traveling Two Different Routes around the Benzene Ring? *J. Phys. Chem. C* **2017**, *121*, 11739–11746.
- (64) Sam-ang, P.; Reuter, M. G. Characterizing Destructive Quantum Interference in Electron Transport. *New J. Phys.* **2017**, *19*, No. 053002.
- (65) Garner, M. H.; Li, H.; Chen, Y.; Su, T. A.; Shangguan, Z.; Paley, D. W.; Liu, T.; Ng, F.; Li, H.; Xiao, S.; Nuckolls, C.; Venkataraman, L.; Solomon, G. C. Comprehensive Suppression of Single-Molecule Conductance using Destructive σ -Interference. *Nature* **2018**, *558*, 415–419.
- (66) Arroyo, C. R.; Tarkuc, S.; Frisenda, R.; Seldenthuis, J. S.; Woerde, C. H. M.; Eelkema, R.; Grozema, F. C.; van der Zant, H. S. J. Signatures of Quantum Interference Effects on Charge Transport through a Single Benzene Ring. *Angew. Chem., Int. Ed.* **2013**, *52*, 3152–3155.
- (67) Nakamura, Y.; Aratani, N.; Osuka, A. Cyclic Porphyrin Arrays as Artificial Photosynthetic Antenna: Synthesis and Excitation Energy Transfer. *Chem. Soc. Rev.* **2007**, *36*, 831–845.
- (68) Ziesel, R.; Harriman, A. Artificial Light-Harvesting Antennae: Electronic Energy Transfer by Way of Molecular Funnel. *Chem. Commun.* **2011**, *47*, 611–631.
- (69) Yang, J.; Yoon, M.-C.; Yoo, H.; Kim, P.; Kim, D. Excitation Energy Transfer in Multiporphyrin Arrays with Cyclic Architectures:

Towards Artificial Light-Harvesting Antenna Complexes. *Chem. Soc. Rev.* **2012**, *41*, 4808–4826.

(70) Manzano, D.; Hurtado, P. I. Symmetry and the Thermodynamics of Currents in Open Quantum Systems. *Phys. Rev. B* **2014**, *90*, No. 125138.